Geometrical Registration of Images: The Multiresolution Approach

Abstract

Geometrical registration of two images is nowadays a current and important step in remote sensing in view of further processing and interpretation of the data. Therefore, geometrical registration of images with different ground resolutions is useful for a better comprehension of dynamic processes (i.e., deforestation, desertification), as well as for extrapolating models of interpretation from a small region to larger areas.

We present a new method of automatic registration, based on a multiresolution decomposition of the images using the wavelet transform. The main properties of this transform, as well as how the use of the wavelet model leads to an automated geometric matching between the different images, are described. Our technique has been applied to different sets of data acquired with the same sensors (SPOT HRV; Landsat MSS) as well as from different sensors with different resolutions (SPOT HRV and Landsat MSS; Landsat TM and SPOT HRV).

Introduction

Image registration of remotely sensed data is a procedure that determines the best spatial fit between two or more images that overlap the same scene, acquired at the same or at a different date, by identical or different sensors. It is an important step, as it is frequently necessary to compare data taken at different times on a point to point basis, for the study of temporal changes for example. Thus, it is required that the new set of data be processed in such a way that its image under an appropriate transform is in a proper geometrical registration with the previous set of data.

The inventory of natural resources and the management of the environment requires a complex and a relevant perception of the objects to be studied (Manière, 1987). Often, a multiresolution approach is essential for the identification of the phenomena studied, as well as for the understanding of the dynamic processes related to them. In this case, the processing of data taken by different sensors with a different ground resolution is necessary.

Another important situation where the need for different images acquired with a different ground resolution sensor arises is when the generalization to larger surface areas of an identification or an interpretation model, based on small areas (Achard and Blasco, 1990). This is the case for studies at the scale of a continent (Justice and Hiernaux, 1986; Hiernaux and Justice, 1986; Tucker *et al.*, 1986). Therefore, the data must be geometrically registered with the best accuracy.

Several digital techniques, such as cross correlation, normal cross correlation, and minimum distance criteria, have been used for the automatic registration of images (Jeansoulin, 1982; Barnea and Silverman, 1972; Pratt, 1974). In this paper, we present a procedure for automatic registration of remotely sensed data based on the multiresolution decomposition of images with the wavelet transform. The advantage of the wavelet transform is that it produces both spatial and frequency information which allows the study of the image by frequency bands. We will illustrate this study with different sets of data obtained with identical sensors as well as with different sensors, and, particularly, the registration of SPOT with SPOT data, Landsat MSS with Landsat MSS data, SPOT with Landsat MSS data, and SPOT with Landsat TM data.

The Wavelet Transform

The Continuous Wavelet Transform

The continuous wavelet transform of a one-dimensional signal $f(x)$ with respect to the analyzing wavelet $\psi(x)$ is the two-dimensional set defined as

$$W(a,b) = \frac{1}{\sqrt{a}} \int_{-\infty}^{+\infty} f(x)\psi^* \left(\frac{x-b}{a}\right) dx \qquad (1)$$

where a is the scale factor. The wavelet coefficients $W(a,b)$ give information on the signal at the location b and for the scale a. The function $\psi(x)$ must obey the admissibility condition: i.e.,

$$C = \int_0^{\infty} \frac{|\hat{\psi}(\omega)|^2}{\omega} d\omega < \infty \qquad (2)$$

It has also been shown (Grossman *et al.*, 1989) that an inversion formula exists: i.e.,

$$f(x) = \frac{1}{C} \int_0^{+\infty} \int_{-\infty}^{+\infty} \frac{1}{\sqrt{a}} W(a,b)\psi\left(\frac{x-b}{a}\right) \frac{da\,db}{a^2} \qquad (3)$$

The wavelet transform can then be easily interpretated in the Fourier space as a set of bandpass filters. The signal is examined both in direct space, pixel by pixel and, in frequency space, band by band. The filtering is determined by the basic wavelet function.

The Discrete Wavelet Transform

In order to process observed images, a discrete approach must be used. Mallat (1989) showed that the wavelet transform can be reduced to the same number of samples as the

Jean-Pierre Djamdji
Ecologie et Phytosociologie, Université de Nice - Sophia Antipolis, Faculté des Sciences, B.P 71 - 06108 Nice Cedex 2, France

Albert Bijaoui
Observatoire de la Côte d'Azur, URA 1361 CNRS A. Fresnel, B.P 139 F-06003 Nice Cedex, France

Roger Maniere
Institut d'Aménagement, Université de Bordeaux III, 33405 - Talence Cedex, France

Photogrammetric Engineering & Remote Sensing, Vol. 59, No. 5, May 1993, pp. 645–653.

0099-1112/93/5905–651$03.00/0

original signal, using the concept of the multiresolution analysis. However, the discrete approach we used was done with the so called *algorithm à trous* (Holdschneider *et al.*, 1989).

THE "ALGORITHM À TROUS"

We assume that the sampled data $\{f_i^{(0)}\}$ are the scalar products at pixel $\{i\}$ of the function $f(x)$ with a given scaling function $\phi(x)$ which corresponds to a low pass filter: i.e.,

$$f_i^{(0)} = <f(x), \phi(x - i)> \tag{4}$$

where $\phi(x)$ must satisfy

$$\frac{1}{2}\phi\left(\frac{x}{2}\right) = \sum_n h(n)\phi(x - n). \tag{5}$$

The first filtering is then performed by a twice magnified scale leading to the $\{f_i^{(1)}\}$ set. The signal difference $\{f_i^{(0)} - f_i^{(1)}\}$ contains the information between these two scales and is the discrete set associated with the wavelet transform corresponding to $\phi(x)$. The associated wavelet $\psi(x)$ is, therefore (Bijaoui, 1991),

$$\frac{1}{2}\psi\left(\frac{x}{2}\right) = \phi(x) - \frac{1}{2}\phi\left(\frac{x}{2}\right) \tag{6}$$

The distance between two samples increasing by a factor of two from the scale $(n - 1)$ to the next one, $f_i^{(k)}$, is given by

$$f_i^{(k)} = \sum_n h(n) f_{i+n2^{k-1}}^{(k-1)} \tag{7}$$

and the discrete wavelet transform $w(i,k)$ by

$$w(i,k) = f_i^{(k-1)} - f_i^{(k)}. \tag{8}$$

The linear piece-wise continuous scaling function was used in our calculations. The algorithm allowing one to rebuild the data frame is the following: we add the last smoothed array $f_i^{(n)}$ to all the differences $w(i,k)k = 1$ to n: i.e.,

$$I_i = f_i^{(n)} + w(i,n) + w(i,n - 1) + \cdots + w(i,1) \tag{9}$$

This works independently of the number of scales. The transformation is overdetermined, no decimation being done as in the pyramidal case and therefore the number of points increases by a factor k. This overdetermination may therefore be useful when we process small data up to some relative high number of scales, 5 or 6, for example. This is our case as a scene may not be as clear of clouds as one would like it to be.

The above *algorithm à trous* is easily extensible to the two-dimensional space. It will then be applied at each step separately in the x and y dimension. The reconstruction algorithm is strictly the same as in the one-dimensional space.

A complete description of the implementation of this algorithm can be found in Bijaoui and Giudicelli (1991).

The Geometrical Study

The Main Steps

Our aim is to register two or more images of the same object field, taken either from the same sensor at different dates, or by different sensors with different ground resolutions at the same or at different dates. However, we must first define a reference frame to which all the other images (if more than two) will be reduced (Castlemen, 1979; Nilblack, 1986). Let us call the image to be warped the input image and the image generated the corrected image. The geometric correction is usually performed by three operations:

- The measure of a set of well defined ground control points (GCP), which are features well located both in the input image and in the reference image.
- The determination of the warping or deformation model, which is usually done by specifying a mathematical deformation model defining the relation between the coordinates (x, y) in the reference image and (X, Y) in the input image.
- The construction of the corrected image with the same parameters as those of the reference frame, but with image values determined in the measured image. This is called an output-to-input mapping.

The main difficulty lies in the automated localization of the corresponding GCP, because the accuracy of their determination will affect the quality of the registration. In fact, there are always ambiguities in matching two sets of points, as a given point corresponds to a small region D, which takes into account the prior geometric uncertainty between the two images, and many objects could be contained in this region.

One property of the wavelet transform is to have a sampling step proportional to the scale. When we compare the images in the wavelet transform space, we can choose a scale corresponding to the size of the region D, so that no more than one object could be detected in this area, and the matching is done automatically.

The Deformation Model

A general model for characterizing misregistration between two sets of remotely sensed data is a pair of bivariate polynomials given by the equations

$$x_i = \sum_{p=0}^{N} \sum_{q=0}^{N-p} a_{pq} X_i^p Y_i^q = Q(X_i, Y_j) \tag{10}$$

$$y_i = \sum_{p=0}^{N} \sum_{q=0}^{N-p} b_{pq} X_i^p Y_i^q = R(X_i, Y_j) \tag{11}$$

where (X_i,Y_i) are the coordinates of the ith GCP in the reference image and (x_i,y_i) the corresponding GCP in the input image. N is the degree of the polynomial. Usually, for images taken under the same *imaging direction*, polynomials of degree one or two are sufficient. We then compute the unknown parameters $(N+1)(N+2)/2$ for each polynomial) using the least mean-square estimator (LMSE).

The Image Correction

One may consider two cases for a geometric registration:

- The registration of images obtained from the same sensor with the same ground resolution and the same *imaging direction*. The registration is then done in the pixel space.
- The registration of images taken by different sensors and having a different ground resolution. The registration is then done in the real coordinates space.

THE PIXEL SPACE

Once the coefficients of the polynomials have been determined, $Q(i,j)$ and $R(i,j)$ are computed, and the output image is generated as follows:

- For each output pixel location (i,j), we compute (k,l), $k = Q(i,j)$ and $l = R(i,j)$, record the pixel value at the location (k,l) and assign it to the output pixel at (i,j). The process is iterated over the entire image and the image output is then generated.
- The pixels values (k,l) are generally not integers, so an interpolation must be done to calculate the intensity value for the

output pixel. Nearest-neighbors, bilinear, bicubic, and spline interpolations are the most widely used.

The Real Space

We transform the coordinates of the GCPs from the pixel space (i,j) to the real space (i_r,j_r) and then compute the coefficient of the polynomials $Q(i_r,j_r)$ and $R(i_r,j_r)$. The output image is then generated as follows:

- Each pixel location (i,j) is transformed into its real coordinates value (i_r,j_r), then $(k_r=Q(i_r,j_r), l_r=R(i_r,j_r))$ is computed. These values are then transformed back into their pixel space value (k,l). We then record the pixel value at (k,l) and assign it to the output pixel at (i,j) as in the pixel space case. The image output is then generated.
- As in the pixel space case, the pixel values (k,l) are generally not integers, so an interpolation must be performed.

Image Registration Using the Wavelet Transform

Registration of Images from the Same Satellite

Let I_n, $n \in (1,N)$, $N \geq 2$, be the images to be processed. Let I_1 be the reference image, and let M be the largest distance in the pixel space between two identical features. From the previous section, it follows that the matching must be first processed with the largest scale L, $2^{L-1} < M \leq 2^L$, in order to automatically match without errors the identical features (Bijaoui and Giudicelli, 1991).

On each image I_n, we compute the wavelet transform with the so called *algorithm à trous* up to the scale L. We then obtain $N \times L$ smoothed image $S_{nl}(i,j)$ and $N \times L$ wavelet images $W_{nl}(i,j)$, $n \in (1,N)$, and $l \in (1,L)$. The smoothed images are not used in the matching procedure. The reference image will be for $n = 1$.

L being the initial dyadic step, we achieve on $W_{nl}(i,j)$ a detection procedure and we keep only the structures above a threshold of $(\theta \times \sigma_{n1})$, θ being a constant which increases when the resolution decreases, and σ_{n1} being the standard deviation of W_{n1}. We only retain from these structures their local maxima which will then play the role of GCP. These points correspond to significant image patterns, and we must find them in each wavelet image corresponding to the same area. Considering that the noise $n(x)$, which is located in the high frequencies, has a Gaussian distribution with a standard deviation of σ, then 99.73 percent of the noise is located in the interval of $[-3\sigma, 3\sigma]$ (Kendal and Stuart, 1973). Therefore, the wavelet image W_{n1} for the first resolution contains the high frequencies of the image and thus contains the noise. By thresholding this image at 3σ, only the significant signal is retained, as 99.73 percent of the noise is eliminated. The algorithm being a dyadic one, the band width is reduced by a factor 2 at each step, so the amount of noise in the signal decreases rapidly as the resolution increases.

For the step L, and for each image $n \in (2,N)$, we compare the positions of the objects detected to the ones found in the reference image W_{1L}. At this step, we can match identical features with confidence, and therefore determine the relationship between the coordinates of the different frames.

Let (ξ_{nl}, η_{nl}) be the position of a maximum for W_{nl}, the matching identifying it as the object m giving a set of coordinates

$$x_{nlm} = \xi_{nl} \quad (12)$$

$$y_{nlm} = \eta_{nl} \quad (13)$$

The deformation model is then calculated by

$$x_{nlm} = Q(X_{1lm}, Y_{1lm}) \quad (14)$$

$$y_{nlm} = R(X_{1lm}, Y_{1lm}) \quad (15)$$

We now consider the wavelet images of order L-1 and detect a new set of maxima in each image. We then transform the coordinates of each maximum detected in the reference image using the previous parameters. That allows us to easily match the maxima and to determine the new parameters of the deformation model.

This process is iterated until the last scale corresponding to the wavelet of the best resolution is reached. The best geometrical correspondence is then established. A polynomial of degree one is used for the first steps, and may eventually be increased to two in the last few steps. The image is then warped using the final coefficients. The flow-chart of this algorithm is given in Figure 1.

Registration of Images of Different Sensors

The registration of images obtained from different sensors with a different ground resolution is done in three steps:

- First the images are reduced to the same ground resolution, generally to that of the lowest one.
- The matching is then done and the deformation model is calculated both in the real and the pixel space.
- The image of higher resolution is then registered in the real coordinate space.

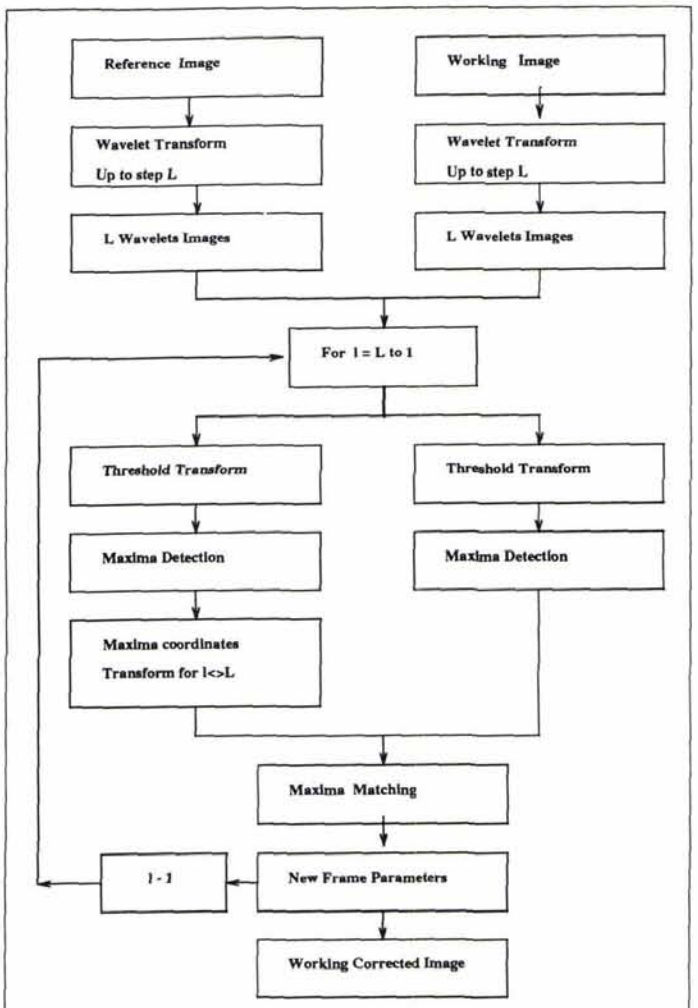

Figure 1. Flow chart of the geometrical registration algorithm.

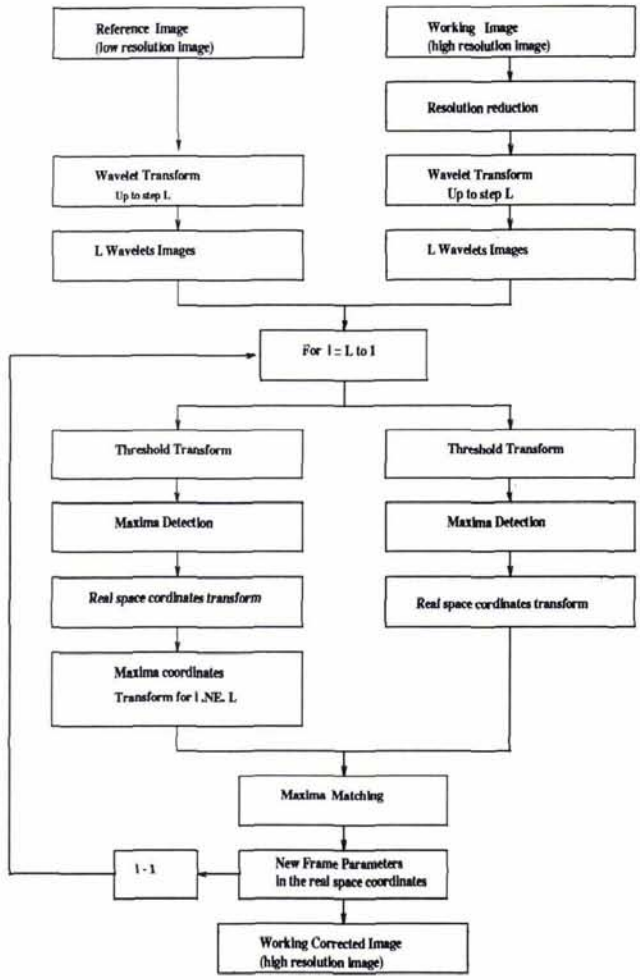

Figure 2. Flow chart of the algorithm for the registration of images obtained from different sensors.

The Reduction to the Same Ground Resolution

We have studied the registration of SPOT with Landsat MSS data and SPOT with Landsat TM data.

- For the SPOT to MSS data, a *pyramidal algorithm* was used up to two scales. The algorithm is the same as the usual one with the difference that one sample out of two is retained in each scale, the data being then reduced by a factor of two at each step.
- For the SPOT to TM data, a different approach was used: The sampled image was assumed to be the result of the scalar product of the continuous image with a scaling function $\phi(x)$, where $\phi(x)$ is the door function. Thus, an analytical approach was used to compute the resulting transformation of SPOT data into TM data. We get

for $k = 2l$

$$n_T(k) = \left\{ n_S(3l) + \frac{1}{4}[n_S(3l-1) + n_S(3l+1)] \right\} \frac{2}{3} \quad (16)$$

for $k = 2l + 1$

$$n_T(k) = \left\{ \frac{3}{4} n_S(3l+1) + n_S(3l+2)] \right\} \frac{2}{3} \quad (17)$$

where n_T is the pixel in the TM image, n_S the pixel in the SPOT image and 2/3 is a coefficient introduced to satisfy flux conservation.

The flow chart of the registration of images obtained from different sensors is given in Figure 2.

Results

For all our scenes, we have extracted subregions of different sizes, in order to avoid (1) working on very large images because this will require lots of disk space; (2) dealing with regions full of clouds or snow, as this is sometimes the case, one could hardly have a scene totally free of clouds or snow in some regions.

The bicubic interpolation was used for the registration.

SPOT Data

The scenes we have worked on are

- Scene No. 51-279, dated 18 May 1989, taken at 10h48m10s, composed of 3005 rows and 3270 columns.
- Scene No. 51-279, dated 12 May 1986, taken at 10h41m28s, composed of 3003 rows and 3253 columns.

These scenes from the region of Ain Ousseira in Algeria were taken with a three-year separation in time in a region subject to desertification and are, therefore, radiometrically very different, as one can easily see. Two sub-scenes of 750 by 750 pixels where extracted in the XS3 band (0.79 to 0.89 μm) which corresponds to the near infrared wavelength. Once these regions were selected, our geometric registration algorithm was applied, using the scene of 1986 as the reference one (Figure 3) and the scene of 1989 as the image to be registered. The processing was done using a six-levels wavelet decomposition. The final registration is given in Figure 4.

Figure 3. The SPOT XS3 reference image.

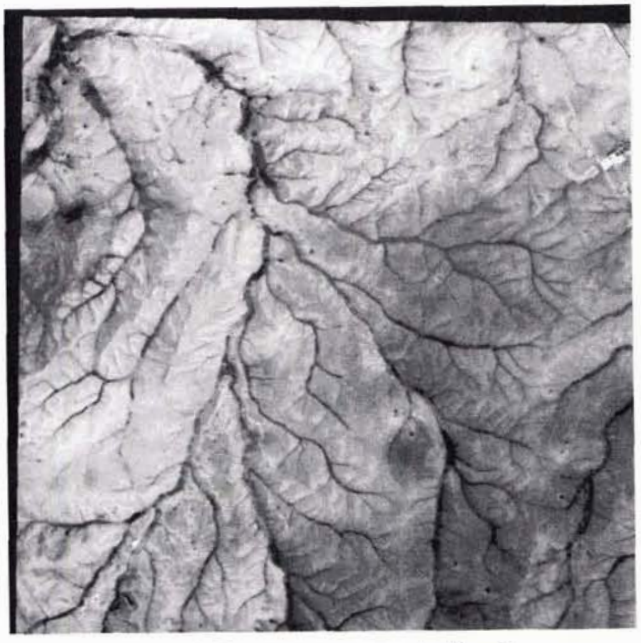

Figure 4. The SPOT XS3 corrected image.

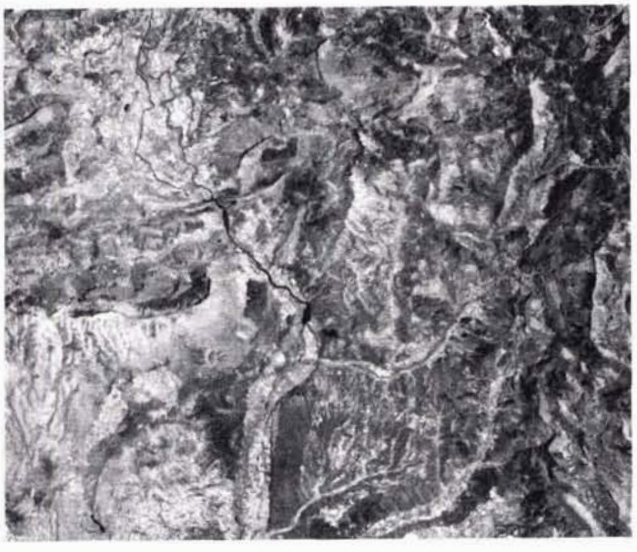

Figure 5. The Landsat MSS3 reference image.

MSS Data

The scenes we have worked on are

- Scene No. 195-29, dated 23 July 1984, composed of 2286 rows and 2551 columns.
- Scene No. 195-29, dated 28 November 1984, composed of 2286 rows and 2551 columns.

These scenes from the region of the Alpes Maritimes in France were taken during the same year but in different seasons and are, therefore, radiometrically different. Two subscenes of 600 by 700 pixels were extracted in the MSS3 band (0.7 to 0.8 μm) which correspond to the near infrared wavelength. The scene of July 1984 was taken as the reference image (Figure 5) and the one from November 1984 as the working image. The processing was done using a six-levels wavelet decomposition. The final registration is given in Figure 6.

SPOT with MSS Data

The scenes we have worked on are

- Scene No. 53-261, dated 24 July 1986, acquired by the HRV of the SPOT satellite in its multispectral bands and composed of 3002 rows and 3140 columns.
- Scene No. 195-29, dated 23 July 1984, acquired by the MSS of

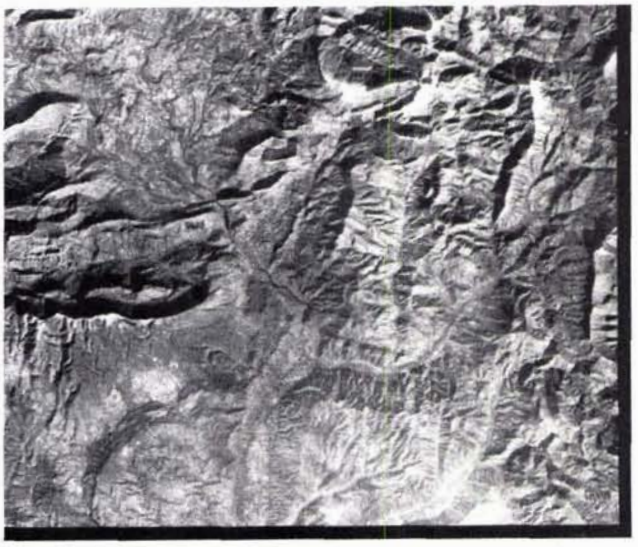

Figure 6. The Landsat MSS3 corrected image.

Figure 7. The Landsat MSS3 reference image.

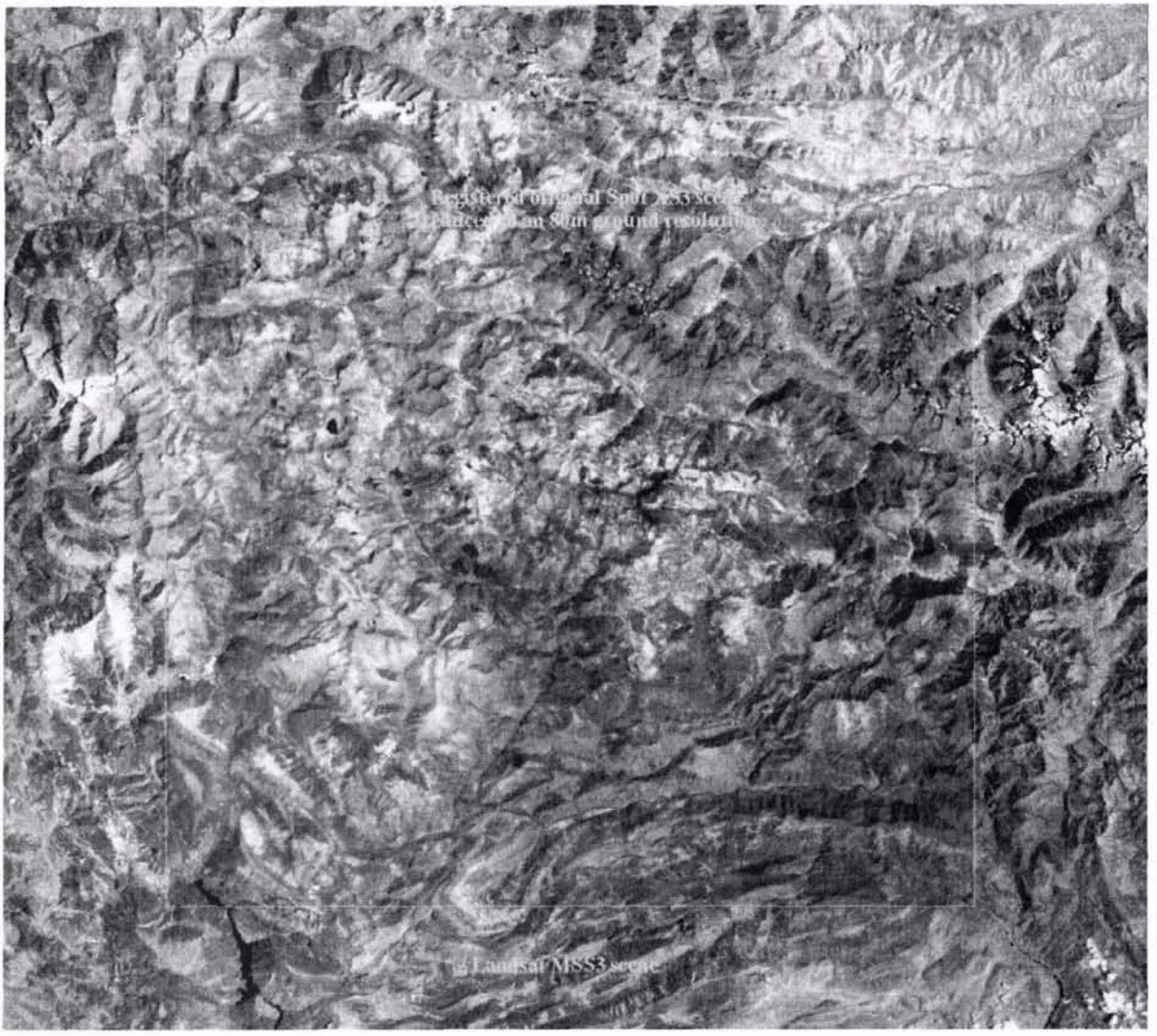

Figure 8. The original registered SPOT image, reduced to an 80-m ground resolution and enlayed into the MSS scene.

the Landsat satellite and composed of 2286 rows and 2551 columns.

These scenes are from the region of the Alpes Maritimes in France. The bands processed were the XS3 for SPOT and the MSS3 for Landsat. The SPOT scene was first reduced to an 80-m ground resolution, then two sub-scenes of 350 by 400 pixels were extracted from the 80-m SPOT and from the MSS3 scenes. Once these regions were selected, our algorithm was applied using the MSS3 scene as the reference one (Figure 7) and the 80-m SPOT scene as the working one. The processing was then done using a six-levels wavelet decomposition. Finally, the original SPOT scene was registered. Once the process done, the rectified original SPOT scene was reduced to an 80-m ground resolution and inlayed in the MSS3 scene in order to evaluate the accuracy of the procedure (Figure 8). Figure 9 shows the SPOT XS3 80-m corrected sub-image.

SPOT with TM Data

The scenes we have worked on are

- Scene No. 195-29, dated 23 July 1984, acquired by the TM of the Landsat satellite and composed of 5760 rows and 6920 columns.
- Scene No. 54-261, dated 24 July 1986, acquired by the HRV of the SPOT satellite in its multispectral bands and composed of 3003 rows and 3142 columns.

These scenes are from the region of the Alpes Maritimes in France. The bands processed were the XS3 for SPOT and the TM4 (0.76 to 0.90 μm) in the near infrared for Landsat. The SPOT scene was first reduced to a 30-m ground resolution, then two sub-scenes of 512 by 512 pixels were extracted from the 30-m SPOT and from the TM4. Once these regions were selected, our algorithm was applied using the TM scene (Figure 10) as the reference one, and the 30-m SPOT

Figure 9. The SPOT XS3 reduced to an 80-m ground resolution output image.

Figure 10.The Landsat TM4 reference image.

scene as the working one. The processing was then done using a 6 level wavelet decomposition. Finally, the original SPOT scene was registered. In Figure 11 we can see the SPOT XS3 30-m corrected image.

SPOT with Different Imaging Directions

The scenes we have worked on are

- Scene No. 148-319, dated 05 February 1991, taken at 07h51m04s, composed of 3000 rows and 3000 columns, level 1a.
- Scene No. 148-319, dated 02 April 1988, taken at 07h34m40s, composed of 3003 rows and 3205 columns, level 1b.

These two scenes from the eastern region of Marib in the

Figure 11.The SPOT XS3 reduced to a 30-m ground resolution output image.

Figure 12. The SPOT 1a input image.

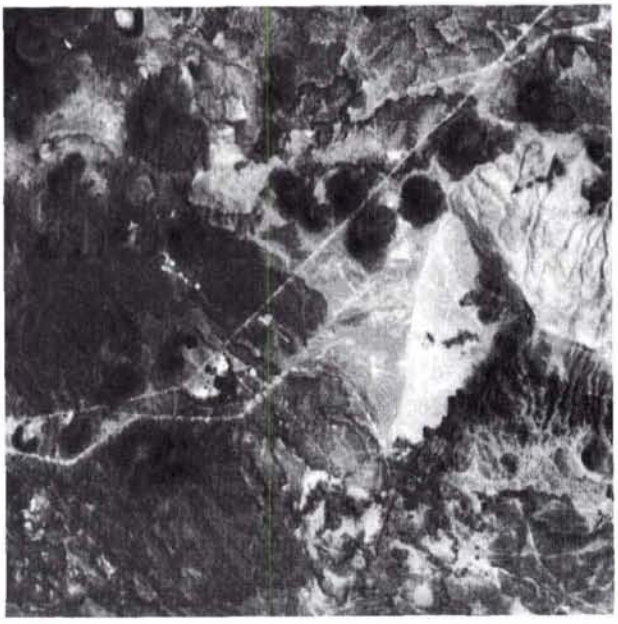

Figure 13. The SPOT 1b reference image.

Figure 14.The SPOT 1a output image.

Republic of Yemen were taken under different imaging directions. The level 1a (Spotimage, 1986) (Figure 12) was taken with an incidence angle of 25.8 degrees left, while the level 1b (Spotimage, 1986) (Figure 13) was taken with an incidence angle of 6.3 degrees right. Two subscenes of 512 by 512 pixels were extracted. An attempt to register these two images was done, using level 1b as the reference image and level 1a as the working image. The registration was globally not very good, especially in the area of mountains (Figure 14). This was due to the polynomial model used, which is inadequate in this case.

TABLE 1. SUMMARY OF THE PRINCIPAL RESULTS FOR THE GEOMETRIC CORRECTION ALGORITHM

Image	Number of GCP	RMSDE (pixel)	RMSDE (m) (real coordinate system)	Processing Time
Spot	327	0.623		15mn
MSS	106	0.559		10mn
SPOT/MSS	108	0.547	69.870 m	20mn
SPOT/TM	628	0.617	19.003 m	24mn
SPOT 1a-1b	329	0.594		6mn

Error Analysis

The criteria used for the evaluation of the registration accuracy was the root-mean-square distance error, given by

$$\text{RMSDE} = \sqrt{\frac{1}{N}\sum_{i=1}^{N} \text{line\_residual}[i]^2 + \text{column\_residual}[i]^2}, \quad (18)$$

N being the total number of ground control points.

The final registration is of good quality, as we reach a subpixel accuracy, the RMSDE being approximately 0.6 for all the cases studied. A subpixel accuracy is also reached for images with different ground resolutions, as the RMSDE evaluated in the real coordinate system is less than the largest ground resolution of the images studied. The registration of images taken at different imaging directions, despite the fact that the RMSDE is 0.594, is of poor general quality, especially in the regions of elevations. This can be explained by the fact that GCPs in these regions have been rejected by the matching procedure as the polynomial used was inadequate for this case.

The processing time gives the time taken by the procedure on a Sparc IPC workstation. This includes the wavelet transform of the images, the matching procedure, and the interpolation of the working image and the image of higher resolution (in the case of images with different ground resolution) with a bicubic convolution.

A summary of the results can be found in Table 1.

Conclusions

We have described a new method for the geometric registration of images with the same as well as with different ground resolution. The procedure is fully automated, the algorithms are fast, and the implementation easy. The main drawback of this algorithm is the large amount of disk space needed for the processing, due to the use of the *algorithm à trous*. The use of Mallat's algorithm or any other pyramidal algorithm may reduce this large amount of disk space, but it will then be difficult to process small images up to a relative high scale due to the reduction of the image size by a factor of two at each step. The polynomial model used for the registration is inadequate for the processing of images taken under a different imaging direction, but is adequate for images taken under the same imaging direction with the same or different ground resolutions.

Acknowledgments

This work was carried out with the financial support of the Programme National de Télédétection Spatiale du CNRS (PNTS 91).

References

Achard, F., and F. Blasco, 1990. Analysis of Vegetation Seasonal Evolution and Mapping of Forest Cover in West Africa with the use of NOAA AVHRR HRPT Data, *Photogrammetric Engineering & Remote Sensing* 56(10):1359–1365.

Barnea, D.I., and H.F. Silverman, 1972. A Class of Algorithms for Fast Digital Image Registration, *IEEE Transactions on Computers* C-21(2):179–186.

Bijaoui, A., 1991. *Algorithmes de la Transformation en Ondelettes—Applications à l'Imagerie Astronomique*, Cours CEA/EDF/INRIA.

Bijaoui, A., and M. Giudicelli, 1991. The Optimal Image Addition Using the Wavelet Transform, *Experimental Astronomy* 1:347–363.

Castleman, K.R., 1979. *Digital Image Processing*, Prentice-Hall Signal Processing Series.

Grossmann, A., R. Kronland-Martinet, and J. Morlet, 1989. *Wavelets, Time-Frequency Methods and Phase Space*, Springer-Verlag, Berlin, pp. 2–20.

Hiernaux, P.H.Y., and C.O. Justice, 1986. Suivi du développement végétal au cours de l'été 1984 dans le Sahel Malien, Intern. Journal of Remote Sensing 7(11):1515–1531.

Holdschneider, M., R. Konland-Martinet, J. Morlet, and P. Tchamitchan, 1989. *Wavelets, Time-Frequency Methods and Phase Space*, Springer-Verlag, Berlin.

Jeansoulin, R., 1982. *Les Images Multi-sources en Télédétection: mise en correspondance numerique et analyse de la structure geometrique*, Thèse Doctorat d'Etat, Université Paul Sabatier, Toulouse.

Justice, C.O., and P.H.Y. Hiernaux, 1986. Monitoring the grasslands of the sahel using NOAA AVHRR data: Niger 1983, *Intern. Journal of Remote Sensing* 7(11):1475–1495.

Kendal, M.G., and A. Stuart, 1973. *The Advanced Theory of Statistics*, Third Edition, Vol. 2., Charles Griffin & Company Limited, London.

Mallat, S., 1989. A Theory for Multiresolution Signal Decomposition: the wavelet representation, *IEEE Trans. Patt. Anal. Mach. Intel.* 11(7):676–693.

Manière, R., 1987. *Télédetection Spatiale et Aéroportée et Systèmes d'Information Géocodées sur l'environnement: principes généraux et étude de quelques domaines d'applications*, Thèse Doctorat d'état, Université Aix-Marseille III.

Nilblack, W., 1986. *An Introduction to Digital Image Processing*, Prentice-Hall International.

Pratt, W.K., 1974. Correlation Techniques of Image Registration, *IEEE Transactions on Aerospace and Electronic Systems* AES-10:353–358.

Spotimage, 1986. *Guide Des Utilisateurs de Données SPOT, Vol. 2, Guide Pratique*, CNES et SPOTIMAGE.

Tucker, C.J., C.O. Justice, and S.D. Prince, 1986. Monitoring the grasslands of the sahel: 1984–1985, *Intern. Journal of Remote Sensing* 7(11):1571–1582.

(Received 16 June 1992; revised and accepted 2 December 1992)